CHIN. PHYS. LETT. Vol. 38, No. 5 (2021) 056101

Revealing the Pressure-Induced Softening/Weakening Mechanism in Representative Covalent Materials

Tengfei Xu(徐腾飞)[1,2], Shihao Zhang(张世亳)[1,2], Dominik Legut[3], Stan Veprek[4], and Ruifeng Zhang(张瑞丰)[1,2*]

[1]*School of Materials Science and Engineering, Beihang University, Beijing 100191, China*
[2]*Center for Integrated Computational Engineering (International Research Institute for Multidisciplinary Science) and Key Laboratory of High-Temperature Structural Materials & Coatings Technology (Ministry of Industry and Information Technology), Beihang University, Beijing 100191, China*
[3]*IT4Innovations, VSB-Technical University of Ostrava, 17 listopadu 2172/15, 708 00 Ostrava, Czech Republic*
[4]*Department of Chemistry, Technical University Munich, Lichtenbergstr 4, D-85747 Garching, Germany*

(Received 19 January 2021; accepted 5 March 2021; published online 2 May 2021)

Diamond, cubic boron nitride (c-BN), silicon (Si), and germanium (Ge), as examples of typical strong covalent materials, have been extensively investigated in recent decades, owing to their fundamental importance in material science and industry. However, an in-depth analysis of the character of these materials' mechanical behaviors under harsh service environments, such as high pressure, has yet to be conducted. Based on several mechanical criteria, the effect of pressure on the mechanical properties of these materials is comprehensively investigated. It is demonstrated that, with respect to their intrinsic brittleness/ductile nature, all these materials exhibit ubiquitous pressure-enhanced ductility. By analyzing the strength variation under uniform deformation, together with the corresponding electronic structures, we reveal for the first time that the pressure-induced mechanical softening/weakening exhibits distinct characteristics between diamond and c-BN, owing to the differences in their abnormal charge-depletion evolution under applied strain, whereas a monotonous weakening phenomenon is observed in Si and Ge. Further investigation into dislocation-mediated plastic resistance indicates that the pressure-induced shuffle-set plane softening in diamond (c-BN), and weakening in Si (Ge), can be attributed to the reduction of antibonding states below the Fermi level, and an enhanced metallization, corresponding to the weakening of the bonds around the slipped plane with increasing pressure, respectively. These findings not only reveal the physical mechanism of pressure-induced softening/weakening in covalent materials, but also highlights the necessity of exploring strain-tunable electronic structures to emphasize the mechanical response in such covalent materials.

DOI: 10.1088/0256-307X/38/5/056101

By virtue of their strongly covalent bonding characteristics, covalent materials exhibit various excellent physical/chemical properties, with tremendous potential for a variety of applications.[1,2] Generally, with respect to electrical conductivity, i.e., as insulators and semiconductors, covalent solids can be classified into two types, corresponding to ultrawide and narrow bandgaps in their electronic structure, respectively. As two typical covalent insulators, diamond and c-BN have been widely used as the main components of superhard cutting, drilling, and polishing tools in the mechanical, petrochemical, and biomedical industries, due to their unique mechanical characteristics,[3−6] i.e., diamond and c-BN are unambiguously defined as intrinsically superhard materials, with Vickers hardness values of between 70–120 GPa and 48–63 GPa, respectively.[7−10] The superhard character of diamond and c-BN is primarily attributable to the three-dimensional covalent network in their structure, indicating that a short, strong covalent bond is crucial to maintaining their high degree of stiffness and hardness/strength. As two prototypical covalent semiconductors, Si and Ge exhibit many similarities to diamond and c-BN (e.g., covalently bonded solids with a cubic structure under ambient pressure).[11−13] Nonetheless, owing to their longer and weaker covalent bonds, the hardness and strength of Si and Ge are several times lower than those of diamond and c-BN. As strong covalent materials with distinct mechanical behaviors, these two

Supported by the National Natural Science Foundation of China (Grant No. 51672015), the National Key Research and Development Program of China (Grant Nos. 2016YFC1102500 and 2017YFB0702100), the 111 Project (Grant No. B17002), and the Fundamental Research Funds for the Central Universities. Dominik Legut was supported by the European Regional Development Fund in the IT4Innovations National Supercomputing Center—Path to Exascale Project (Grant No. CZ.02.1.01/0.0/0.0/16 013/0001791), within the Operational Programme for Research, Development and Education, and by the Large Infrastructures for Research, Experimental Development, and Innovation Project (Grant No. e-INFRA CZ-LM2018140) by the Ministry of Education, Youth, and Sport of the Czech Republic.
*Corresponding author. Email: zrf@buaa.edu.cn
© 2021 Chinese Physical Society and IOP Publishing Ltd

types of covalent material have garnered much scientific attention and interest; as such, a series of comparative investigations have been conducted over recent decades.[14−16]

Although many experimental and theoretical studies have been performed with respect to the mechanical properties of these two types of covalent material under ambient conditions, leading to a basic understanding of their mechanisms, the mechanical responses of these materials under harsh service environments, e.g., high pressure, have yet to be explored; this area requires consideration, given increasingly rigorous service conditions. For example, a recent study has reported record-setting ultrahigh static pressures generated in diamond anvil cells (DACs) of as much as 495 GPa.[17] In terms of superhard materials such as diamond, it is believed that the metallization of its covalent bonds generally results in a decrease in strength.[8,18−20] One naturally wonders whether a high pressure environment would affect the nature of its covalent bonds, and, consequently, its mechanical properties? Previous studies related to the high-pressure mechanical responses of diamond and c-BN have tended to focus on their elastic properties,[16,21,22] describing a reversible response to external forces within a given elastic limit. It has been observed that these elastic properties are derived from equilibrium structures with small strain, whereas the mechanical properties of a real material is determined by crystal plasticity, which links two plasticity-relevant parameters, i.e., ideal strength, and Peierls stress, corresponding to the electronic instability under large strain, and the lattice-resistance of dislocation slip, respectively.[7,23] By introducing these two plasticity-relevant parameters, Zhang *et al.*[23] calculated the ideal strength and Peierls stress along the weakest shear path of γ-B_{28}, which was originally suggested as another superhard material based on the results of hardness modeling.[24,25] However, the theoretical results showed that both its ideal strength and Peierls stress were much lower than those of diamond, verifying that γ-B_{28} cannot be ranked as an intrinsically superhard material, further confirming the necessity for new mechanical descriptors beyond the widely used hardness model based on equilibrium parameters. Combining elastic properties with plasticity-relevant parameters, Zhang *et al.*[18] performed high-throughput screening of superhard carbon and boron nitride allotropes, and successfully revealed a new superhard carbon allotrope, tI12-C, showing that these two plasticity-relevant parameters, rarely included in previous studies, play a key role in characterizing the mechanical properties of superhard materials, particularly in the context of harsh service environments, such as high pressure.

In addition, both fine processing and servicing in harsh environments, which are usually required for Si- and Ge-based products, may also cause very high local pressure. Therefore, as mentioned above, plastic behaviors, in particular the ideal strength and Peierls stress of Si and Ge under pressure must be carefully considered, since phase transition in Si and Ge can be induced by relatively low pressure (i.e., the phase transition pressures from the cubic diamond phase to a body-centered tetragonal β-tin structure in Si and Ge are about 11.7 and 9.7 GPa, respectively[26,27]), eventually leading to device failure. Umeno *et al.*[28] calculated theoretical shear stress as a function of applied pressure in diamond and Si. They showed that in diamond, the ideal shear strength is increased by compression, which is in good agreement with the hard-sphere model.[29] However, an inverse behavior was observed for Si, where the shear stress decreases under compression. In order to further examine these completely different phenomena in diamond and Si, Pizzagalli *et al.*[15] investigated the dislocation mobility of these two materials under pressure (i.e., Peierls energies as a function of applied pressure). They demonstrated that with increasing pressure, the Peierls energies for both the shuffle-set and glide-set planes of diamond increased. For Si, only the Peierls energies of the glide-set plane increased, while that of the shuffle-set plane decreased with increasing pressure. A further nudged elastic band (NEB) calculation illustrated that, for diamond, both the energy barriers along shuffle-set and glide-set planes increased with increasing pressure, while the energy barrier of Si along the shuffle-set (glide-set) plane decreases (increases) as a function of applied pressure. This work suggests that slip systems in different covalent materials could become softer or harder under applied pressure, indicating that the evident effect of pressure on the mechanical response of these materials. Nonetheless, an analysis of their electronic structure under pressure, has not yet been performed in this or any other previous studies, although it is essential to a deeper understanding of their mechanical behaviors.

In this study, taking diamond, c-BN, Si, and Ge as representative covalent materials, we systematically investigate their elastic responses and plastic behaviors within pressure ranges of 0–500 GPa (for diamond and c-BN) and 0–10 GPa (for Si and Ge). These findings provide a comprehensive overview of the mechanical behaviors of these materials under pressure, and reveal the physical origin of the pressure effect via an in-depth analysis of their electronic structure, providing a thorough approach to understanding the mechanical behaviors of such covalent materials in harsh service environments. Next, we introduce the first-principles calculation method, the approach to calculate elastic properties and ideal strengths, and the semidiscrete variational Peierls–Nabarro model used

to determine Peierls stress. Then, the results of our calculations are presented and discussed. Finally, we summarize this work, and draw our main conclusions.

Methods. First-principles calculations based on density functional theory (DFT) in this work are performed using the Vienna *ab initio* simulation package (VASP)[30] in conjunction with the projector argument wave (PAW) method;[31] the local density approximation (LDA) in the form of Ceperley–Alder[32,33] is adopted as the exchange-correlation functional. We chose a Gaussian method[34] with a smearing width of 0.01 eV for the electronic self-consistency, in which the energy convergence criterion is set at 10^{-6} eV/cell, and all forces acting on atoms are lower than the force convergence criterion, 10^{-3} eV/Å, in ionic relaxation. A plane-wave kinetic energy cutoff of 520 eV, and Monkhorst–Pack k mesh[35] $7\times5\times1\Gamma$-centered grids are used when calculating the generalized stacking fault energy (GSFE). For regular calculations, such as structural optimization and ideal strength calculation, high precision $23\times23\times23$ k-point grids are adopted. Calculations under pressure are employed by switching on the PSTRESS parameter in VASP. The phonon dispersions are calculated by means of PHONOPY code,[36] based on the nonvanishing Hellman–Feynman forces within the harmonic approximation. More specifically, the finite displacement method is employed, and the phonon frequencies and eigenvectors are obtained from the dynamical matrices, which are built based on the calculated force constant. The crystal orbital Hamilton population (COHP) is calculated via LOBSTER code,[37,38] which processes analytic projections from plane-wave and PAW wavefunctions with respect to chemical bonding analysis in solids.[39–41] In order to obtain reasonable chemical bonding information, it is important to ensure that the charge-spilling upon projection is no more than 2%.

The energy-strain method is used to calculate the elastic properties *via* our developed AELAS code,[42] and the lattice constants, along with polycrystalline shear ($G_{\rm VRH}$) and bulk ($B_{\rm VRH}$) moduli, are calculated using the Voigt–Reuss–Hill (VRH) approximation.[43,44] Generally, two different types of deformation are adopted in the first-principles calculations, i.e., affine and alias, corresponding to uniform and localized strains, respectively. This approach has been widely adopted in order to investigate the mechanical response of a given material under strain.[7,45] In this study, the anisotropic ideal tensile and shear strength via affine deformation, and GSFE via alias-shear deformation are calculated using our developed ADAIS code.[45] In order to obtain complete profiles of GSFE, including unstable stacking fault energy (USFE), only vertical movement normal to the slip plane is permitted during atomic relaxation. Further detail relating to this process can be found in our previous studies.[46–48]

The Peierls stress is obtained using our developed PNADIS code,[49] employing the Peierls–Nabarro (P-N) dislocation model, in which the total energy of a dislocation, $E_{\rm total}$, is contributed by two parts of elastic energy $E_{\rm elastic}$, and misfit energy, $E_{\rm misfit}$, i.e., $E_{\rm total} = E_{\rm elastic} + E_{\rm misfit}$, expressed in detail as follows:[50]

$$E_{\rm total} = -\frac{K}{4\pi}\int_{-\infty}^{\infty}\int_{-\infty}^{\infty}\rho(x)\rho(x')\ln|x-x'|dxdx' + \int_{-\infty}^{\infty}\gamma[u(x)]dx, \tag{1}$$

where the elastic energy factors $K = G/(1-\nu)$ relate to edge dislocation, and $K = G$ to screw dislocation; G, and ν represent the shear moduli and Poisson's ratio, respectively, and the misfit density $\rho(x) \equiv du(x)/dx$. Note that the unknown disregistry vector, $u(x)$, in Eq. (1) can be determined by solving the equation $\delta E_{\rm total}/\delta u = 0$,[51] corresponding to the balance of elastic resistance, $F_{\rm EL}$, with restoring force, $-\nabla\gamma[u(x)]$, leading to

$$\frac{K}{2\pi}\int_{-\infty}^{\infty}\rho(x')\frac{1}{x-x'}dx' = -\nabla\gamma[u(x)]. \tag{2}$$

By inserting the disregistry function, which can realistically be described by the trial function,

$$u(x) = \frac{b}{2} + \frac{b}{\pi}\sum\nolimits_{i=1}^{N}\alpha_i \arctan\frac{x-d_i}{\omega_i}, \tag{3}$$

into the left-hand side of Eq. (2), the elastic resistance can be determined first. Subsequently, the variational constants α_i, d_i, ω_i, and c_i are determined by a least-square minimization of the difference between $F_{\rm EL}$ and $\gamma[u(x)]$.[50] Taking account of the discrete nature of the crystalline lattice, when the dislocation locates at position ε, the misfit energy can be rewritten as[52]

$$E_{\rm misfit}(\varepsilon) = \sum\nolimits_{m}\gamma[u(m\Delta x-\varepsilon)]\cdot\Delta x, \tag{4}$$

where Δx is defined as the shortest distance between two equivalent atomic rows in the absence of a dislocation. Accordingly, the Peierls stress $\tau_{\rm P}$ is determined by the derivative of misfit energy:[52]

$$\tau_{\rm P} = \max\left\{\frac{1}{b}\frac{dE_{\rm misfit}(\varepsilon)}{d\varepsilon}\right\}. \tag{5}$$

Generally, two inequivalent {111} slip planes correspond to four groups of 1/2 ⟨110⟩ full dislocation in diamond, i.e., shuffle(glide)-set 0° dislocation, and shuffle(glide)-set 60° dislocation;[15,48,53] this is similar to the case for c-BN, Si, and Ge. In contrast to 1/2 ⟨110⟩ glide-set full dislocation, which can disassociate into two 1/6 ⟨11$\bar{2}$⟩ glide-set partial dislocations, 1/2

⟨110⟩ shuffle-set full dislocation cannot disassociate into partial dislocations, since there is no stable stacking fault along the $[11\bar{2}]$ direction. As regards the determination of the Peierls stress for 1/2 ⟨110⟩ glide-set full dislocation, which dissociates into two 1/6 $\langle 11\bar{2}\rangle$ glide-set partials, we adopt the method proposed by Kamimura,[54] which offers proven reliability.[48,55]

Table S1 shows the calculated lattice constants, elastic properties, and plasticity-relevant parameters of diamond, c-BN, Si, and Ge under atmospheric pressure, all of which are in very good agreement with previous theoretical and experimental results, indicating the rationality of all the methods used in this work.

Results and Discussion: A. Effect of Pressure on Elastic Properties. Firstly, the dynamical stability of these materials is evaluated. As shown in Fig. S1 in the Supplemental Materials (SM), the absence of imaginary modes across the whole Brillouin zone confirms all these materials to be dynamically stable under zero and high pressures. The elastic properties are of fundamental importance in relation to crystalline materials, as they are related to other mechanical properties; below, we evaluate the elastic properties of these materials at different pressures in detail. The shear ($G_{\rm VRH}$) and bulk ($B_{\rm VRH}$) moduli, which describe the resistance to external deformation[8,42,47] of these materials under different pressures are shown in Figs. 1(a) and 1(d). As expected, $B_{\rm VRH}$ increases linearly with pressure, in accordance with the common physical equation ($B = \Delta P/\Delta V$), in which $B_{\rm VRH}$ is proportional to applied pressure. Thus, the $B_{\rm VRH}$ of diamond and c-BN dramatically increases at the same B' (pressure derivative of $B_{\rm VRH}$) of about 2.9 (from 468 to 1911 GPa and 403 to 1847 GPa, respectively). A similar linear increasing trend is also observed in Si and Ge, where the $B_{\rm VRH}$ increased from 97 to 137 GPa, and 72 to 117 GPa (the corresponding B' are about 4.0 and 4.9), respectively. As a comparison, the $G_{\rm VRH}$ indicates the same behavior for all of the materials considered here under applied pressure, i.e., a near-linear increase with a much lower slope, as compared with their corresponding $B_{\rm VRH}$. The substantial variations in the Zener anisotropy factor, $A = 2C_{44}/(C_{11} - C_{12})$,[56] under applied pressures, as shown in Figs. 1(b) and 1(e), demonstrate that the crystalline elastic anisotropy of these materials is very sensitive to pressure.

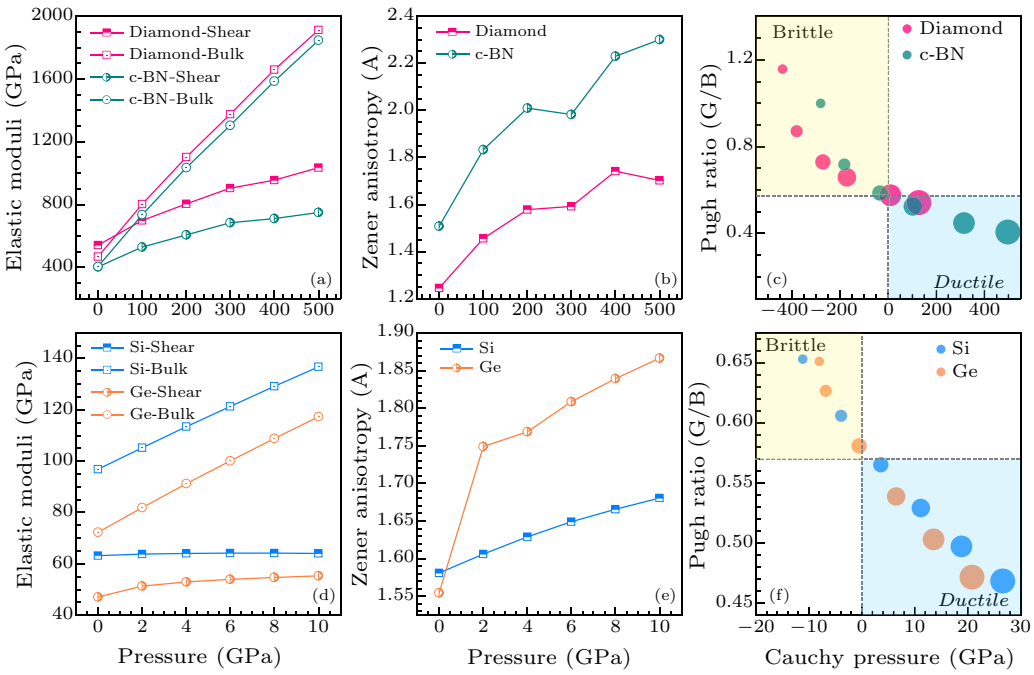

Fig. 1. Variations in elastic moduli, anisotropy index, and Pugh ratio for (a)–(c) diamond and c-BN, together with (d)–(f) Si and Ge under zero and high pressures. The size of the bubbles in (c) and (f) is consistent with the magnitude of pressure.

Taking into account that brittleness and ductility signify two different mechanical behaviors in solids subjected to stress, here, the intrinsic ductility/brittleness criterion, i.e., the Pugh ratio ($G_{\rm VRH}/K_{\rm VRH}$) as a function of Cauchy pressure ($C_{12}-C_{44}$), is introduced to reveal the brittle (ductile) nature of each material.[8,42,47] As shown in Figs. 1(c) and 1(f), the Pugh ratio decreases, while the Cauchy pressure increases with increasing pressure in all cases. Two areas depicted in yellow (blue), representing a Pugh ratio > 0.57 (< 0.57) with a Cauchy pressure < 0 (> 0) suggest the brittle (ductile) nature of the

materials. It is found that the brittle-ductile transition occurs at a pressure of 400 GPa (300 GPa) for diamond (c-BN) and 4 GPa (6 GPa) for Si (Ge), respectively, demonstrating a pressure-enhanced ductility behavior.

B. Pressure-Induced Mechanical Softening/Weakening under Uniform Strain. Figure 2 illustrates the calculated stress-strain curves of diamond, c-BN, Si and Ge along the weakest tensile [111] and shearing (111)[11$\bar{2}$] paths under different pressures, and the corresponding ideal strength vs pressure curves are presented in Figs. 3(a) and 3(c). It is found that the tensile strength of all these materials exhibits an upward trend with increasing pressure, whereas there are noticeable differences in shear strength. With regard to diamond along its shear deformation, although the shear strength increases with the increasing pressure, a turning point appears in the stress-strain curves under applied pressure compared with those under zero pressure, suggesting a pressure-induced softening phenomenon.[18] A similar softening behavior is found in c-BN, where the stress decreases smoothly after reaching critical strain under high pressure, rather than dropping suddenly under zero pressure. Moreover, the highest shear strength of c-BN is achieved at a pressure of 200 GPa, and higher pressures give rise to a decrease in strength. In order to distinguish between this behavior and pressure-induced softening, we define this behavior, whereby strength continuously declines with increasing pressure, as pressure-induced weakening. With regard to Si and Ge, we find only pressure-induced weakening without any strengthening effect, as shown in previous research,[15,28] i.e., similarly to the strength variation in c-BN once the pressure exceeds 200 GPa, the ideal shear strength decreases continuously with increasing pressure.

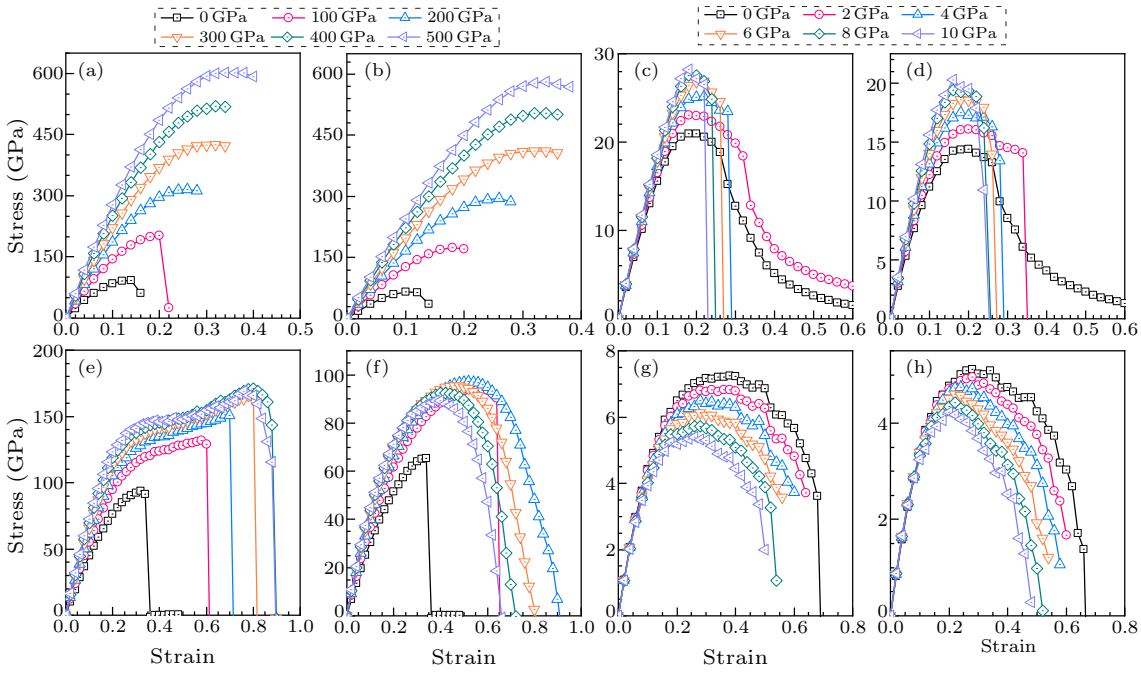

Fig. 2. Calculated stress-strain curves along the weakest tensile [111] and shearing (111)[11$\bar{2}$] path of [(a), (e)] diamond, [(b), (f)] c-BN, [(c), (g)] Si, and [(d), (h)] Ge under zero and high pressures, respectively.

To underline the electronic origin of pressure-induced softening/weakening in diamond, c-BN, Si, and Ge during shear deformation, the valence charge density difference (VCDD) under different strains is calculated. We observe that, in the case of diamond, as compared with its behavior under zero pressure, abnormal charge depletion regions, every two of which stand opposite to each other, with an angular polyhedron shape, appear at a pressure of 100 GPa [see the red arrow in Fig. 3(b4)]. As the strain increases, the abnormal charge depletion region spreads into a spindle-like shape, and finally a willow-like shape, vertically between C–C bonds, at the critical strain ($\gamma = 0.58$) [see Fig. 3(b5–b6)]. Such charge depletion is responsible for the discontinuities in the stress-strain curves, thereby resulting in mechanical softening. With an increase in pressure, the charge accumulation/depletion increases simultaneously, and the evolution of abnormal charge depletion regions under applied strain is basically the same as that found under 100 GPa [see Figs. 3(b7)–(b9) and Fig. S2(a1–a9) in the SM]. For c-BN, a similar abnormal charge depletion region is found at the pressure of 100 GPa, in addition to a change in shape, i.e., a contracted tetra-

hedron shape at zero strain, and gradual splitting into three individual parts until the point of critical strain ($\gamma = 0.56$) [see red circles in Fig. S2(b1–b3) in the SM]. With the pressure increasing to 200 GPa, which corresponds to the stage where the ideal strength increases, no obvious change is observed in the abnormal charge depletion regions under critical strain [see the red circle in Fig. 3(c6)]. However, a significant variation appears when the pressure reaches 300 GPa, i.e., three individual parts conjoin to form a flat triangular prism-like shape at the point of critical strain ($\gamma = 0.46$), compared with the shapes formed under 100 and 200 GPa [see the red circle in Fig. 3(c9)], which accounts for the transition from mechanical softening to weakening above 200 GPa. Since there is no obvious change in the VCDD of Si and Ge across the entire pressure range [see Fig. S2(c1–d9) in the SM], we evaluate the density of state (DOS) of Si and Ge at the Fermi level under a critical strain of 0.12 at different pressures. It is evident that the DOS at the Fermi level of Si and Ge are primarily derived from p orbitals, whose values increase with increasing pressure [Fig. 3(e)], indicating enhanced metallization at the Fermi level. This results in the weakening of the bonds of Si and Ge, and causes a further linear reduction in mechanical strength.

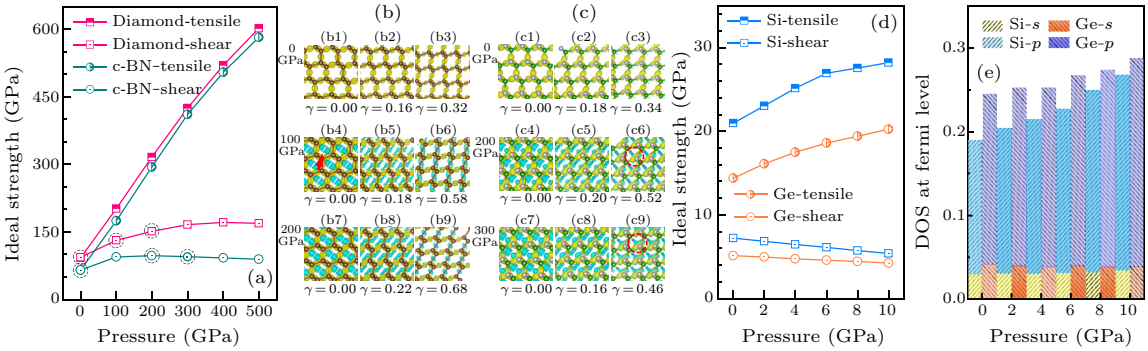

Fig. 3. Variations in ideal strength for (a) diamond and c-BN, together with (d) Si and Ge under different pressures. Calculated isosurfaces of the VCDD of (b1)–(b9) diamond and (c1)–(c9) c-BN under different strains along the $(111)[11\bar{2}]$ shearing path at zero and high pressures. The unit of VCDD is electrons/Bohr^3, and an identical isosurface level of ± 0.022, ± 0.022, and ± 0.0265 electrons/Bohr^3 is used for diamond at 0, 100, and 200 GPa, ± 0.022, ± 0.026, ± 0.0295 is used for c-BN at 0, 200, and 300 GPa, respectively. The blue and yellow regions signify the states of charge depletion (negative) and accumulation (position), respectively. (e) DOS at the Fermi level of Si and Ge, under a strain of 0.12 at different pressures.

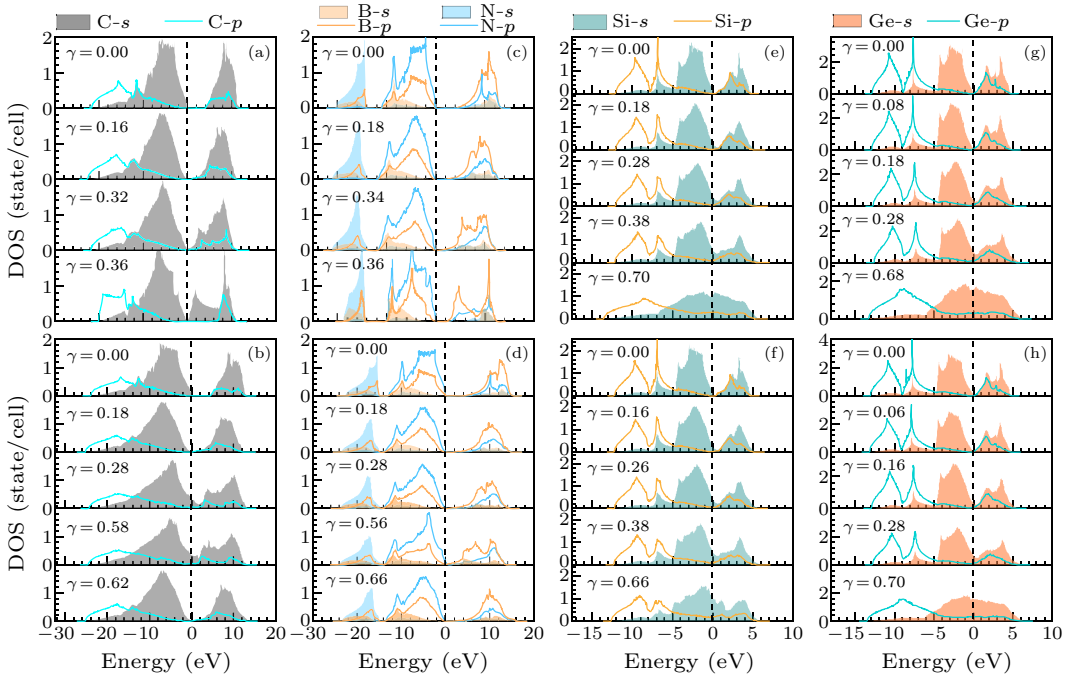

Fig. 4. Calculated DOS of [(a), (b)] diamond, [(c), (d)] c-BN, [(e), (f)] Si and [(g), (h)] Ge under various strains along the $(111)[11\bar{2}]$ shearing path at different pressures (0 and 100 GPa for diamond and c-BN, 0 and 2 GPa for Si and Ge, respectively). The Fermi level is set to zero.

To gain an in-depth understanding of electronic origin, the DOS of diamond, c-BN, Si and Ge are calculated under various strains, at zero and high pressures, and the results are presented in Fig. 4. It is demonstrated that the pressure-induced softening in diamond is attributable to the states increasing at the Fermi level [Figs. 4(a) and 4(b)], resulting in the metallization of the C–C covalent bond. Similarly, graphitization of the electronic structure results in pressure-induced softening/weakening in c-BN, i.e., the bandgap is completely closed until the instability occurs under zero pressure, while the strain ($\gamma = 0.28$) as the band gap reduces to zero is far below the critical strain ($\gamma = 0.56$) at a pressure of 100 GPa. In contrast to the results for diamond and c-BN, strain-induced metallization is observed in Si and Ge at zero pressure [Figs. 4(e) and 4(g)], indicating their intrinsically low stiffness and strength characteristics. Since the variation of DOS in Si and Ge is not obvious from zero to high pressure [Figs. 4(e)–4(h)], the DOS at the Fermi level under a certain strain ($\gamma = 0.12$) is introduced to illustrate the pressure-induced weakening mechanism, as discussed above.

C. Pressure-Induced Shuffle-Set Plane Softening/Weakening under Localized Strain. Inhomogeneous deformation is governed by localized strain, under which the mechanical behavior of a material is much closer to real-life service conditions than under uniform strain.[23] We therefore explore the dislocation-mediated plastic resistance of diamond, c-BN, Si and Ge.

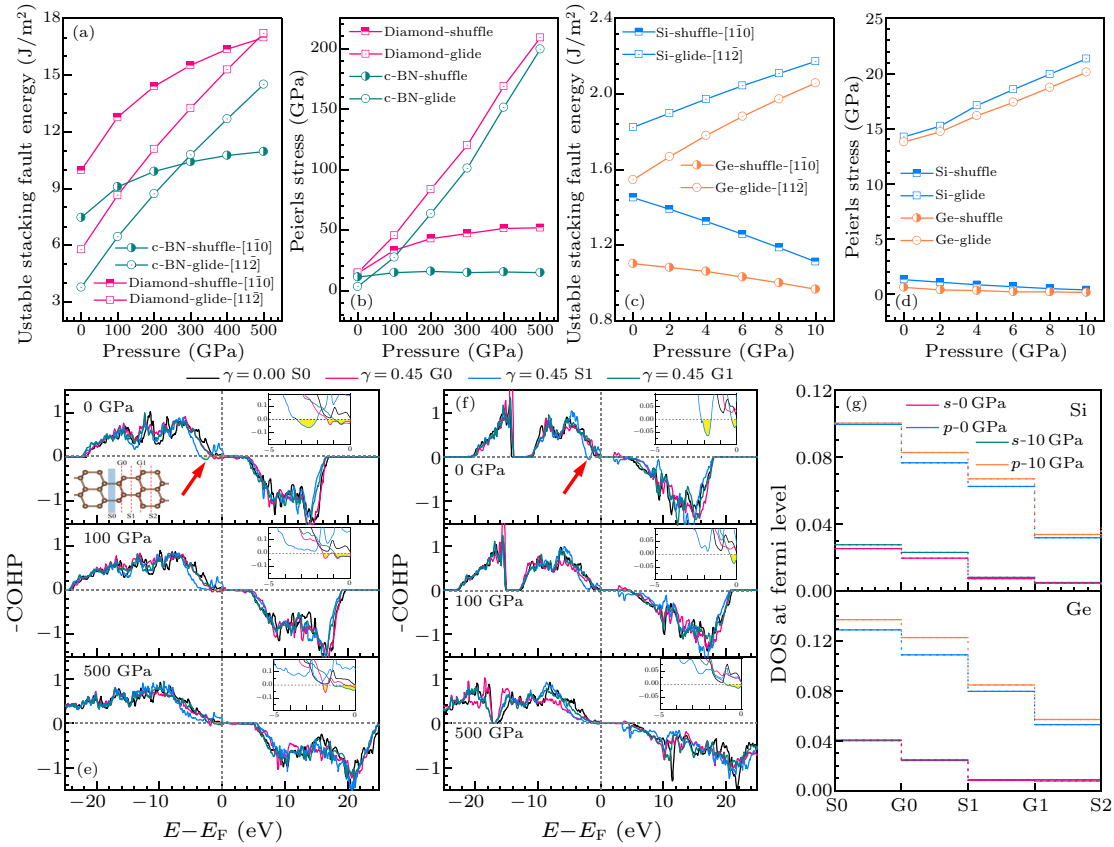

Fig. 5. Calculated USFE and Peierls stress of [(a), (b)] diamond and c-BN, together with [(c), (d)] Si and Ge under different pressures. The COHP curves of the bonds around the slip plane S0 in (e) diamond and (f) c-BN under different displacements ($\gamma = 0.00$ and $\gamma = 0.45$) and at different pressures. (g) DOS values at the Fermi level of each atom in Si and Ge, under a displacement of 0.45, at 0 and 10 GPa.

Figures 5(a) and 5(b) illustrate the unstable stacking fault energy (γ_{US}) and the corresponding Peierls stress (τ_P) of diamond and c-BN vs pressure on the shuffle-set ($\gamma_{US-glide-[11\bar{2}]}$ and $\tau_{P-glide-[11\bar{2}]}$) and glide-set ($\gamma_{US-shuffle-[1\bar{1}0]}$ and $\tau_{P-shuffle-[1\bar{1}0]}$) planes. It is clear that the dependence of $\gamma_{US-glide-[11\bar{2}]}$ and $\tau_{P-glide-[11\bar{2}]}$ on the applied pressure follows a linear relationship, while unprecedented shuffle-set plane softening appears in both diamond and c-BN, i.e., the increase in $\gamma_{US-shuffle-[1\bar{1}0]}$ and $\tau_{P-shuffle-[1\bar{1}0]}$ is much smoother than their corresponding glide-set plane with enhanced pressure. In consequence, the plastic deformation in diamond is always dominated by shuffle-set plane slip, regardless of zero or high pressure, i.e., $\tau_{P-shuffle-[1\bar{1}0]}$ is lower than $\tau_{P-glide-[11\bar{2}]}$ across the entire pressure range. Mean-

while, competition occurs between these two slip systems in c-BN, resulting in the transformation of the dislocation slip mechanism: glide-set plane slip-dominated plastic deformation under zero pressure ($\tau_{\mathrm{P-shuffle-[1\bar{1}0]}} = 1.03$ GPa, which is higher than $\tau_{\mathrm{P-glide-[11\bar{2}]}} = 0.57$ GPa) turns into shuffle-set plane slip-dominated deformation under high pressure (e.g., $\tau_{\mathrm{P-shuffle-[1\bar{1}0]}} = 1.16$ GPa, which is lower than $\tau_{\mathrm{P-glide-[11\bar{2}]}} = 1.43$ GPa under 100 GPa). In order to further explore the underlying atomic mechanisms for pressure-induced shuffle-set plane softening in diamond, we first calculated the fat band structures and the corresponding DOS of diamond slipping at various displacements ($\gamma = 0.00$, 0.45) along the shuffle-set plane, at different pressures. As shown in Fig. S3 in the SM, after 0.45 displacement of slip at 0 GPa, compared with that without slippage ($\gamma = 0.00$), the band gap is completely closed, and hybrid band states (conduction bands) occur, comprising s (red line) and p (blue line) orbitals crossing the Fermi level [Fig. S3(b)], indicating the strain-induced metallic nature of deformed diamond. Moreover, such hybrid states tend to proliferate with increasing pressure [see Figs. S3(d) and 3(f)]. Since the localized strain usually affects several layers of atoms near the defect (i.e., the stacking fault plane in this work) directly, rather than the entire system, the COHP of the bonds around the slip plane of diamond and c-BN are calculated for the purpose of characterizing their softening mechanism more accurately. As shown in Figs. 5(e) and 5(f), for diamond under zero pressure, as slippage occurs in shuffle-set plane S0 [see the topological structure inset in Fig. 5(e)], we find antibonding states under the Fermi level in G0, S1, and G1 planes (see the inset partial view with filled yellow slashed line), and similar antibonding states are observed in c-BN. It is believed that these antibonding states lead to high energy in the slipped structure, with concomitant high SFEs and Peierls stress. However, when diamond and c-BN are subjected to 100 and 500 GPa, the antibonding state in the S1 plane disappears, resulting in a slow increase in unstable stacking fault energy and Peierls stress with increasing pressure, i.e., the softening of the S0 shuffle-set plane. Unlike diamond and c-BN, $\gamma_{\mathrm{US-shuffle-[1\bar{1}0]}}$ and the corresponding $\tau_{\mathrm{P-shuffle-[1\bar{1}0]}}$ of Si (Ge) constantly decrease from 1.30 GPa (0.60 GPa) to 0.34 GPa (0.16 GPa) as pressure increases [Figs. 5(c) and 5(d)], suggesting a pressure-induced weakening behavior, in accordance with Pazzagalli's research.[15] As there are no obvious antibonding states below the Fermi level on G0, S1, or G1 for either Si or Ge, and their COHP curves do not change with increased pressure (see Fig. S4 in the SM), we calculate the DOS at the Fermi level of several layers near the S0 plane under zero and 10 GPa. It is apparent that the DOS at the Fermi level for both Si and Ge are mainly attributable to p orbitals. In addition, the values of DOS at the Fermi level for all bonds around S0 plane increase below 10 GPa, as compared with those under zero pressure, indicating that a higher pressure causes a more profound metallization of the slipped structure, i.e., the weaker bonds around the slipped plane under higher pressure result in pressure-induced weakening of the S0 shuffle-set plane.

In summary, based on several mechanical criteria, we have performed comprehensive investigations of the effect of pressure on the mechanical properties of four representative strong covalent materials, i.e., diamond, c-BN, Si, and Ge, by means of first-principles calculations. Several key findings are given as follows:

(1) The elastic properties of all these materials are found to be very sensitive to pressure; in particular, all of them exhibit a pressure-enhanced ductility.

(2) The pressure-induced softening/weakening under uniform strain exhibits distinct characteristic trends when comparing diamond and c-BN, i.e., abnormal charge-depletion, accompanied by metallization, gives rise to mechanical softening in diamond, whereas the expansion of abnormal charge depletion under 300 GPa leads to a transition from mechanical softening to weakening in c-BN. A similar weakening trend is also found in Si and Ge, accompanied by a pressure-promoted DOS at the Fermi level at the same strain, i.e., higher pressure gives rise to a more profound metallization transition of covalent bonds.

(3) Unprecedented pressure-induced shuffle-set plane softening/weakening is observed in all of the materials under consideration; specifically, the reduction in antibonding states below the Fermi level at high pressures causes shuffle-set plane softening in diamond and c-BN, whereas for Si and Ge, the pressure-induced shuffle-set plane weakening is attributable to the increasing metallization and the corresponding weaker bonds around the slipped plane with the increasing pressure.

References

[1] Karch K, Dietrich D, Windl W, Pavone P, Mayer A P and Strauch D 1996 *Phys. Rev. B* **53** 7259

[2] Zhang Y, Sun H and Chen C F 2005 *Phys. Rev. Lett.* **94** 145505

[3] Jenei Z, O'Bannon E F, Weir S T, Cynn H, Lipp M J and Evans W J 2018 *Nat. Commun.* **9** 1

[4] Semenic T, Hu J, Kraemer S, Housley R and Sudre O 2018 *J. Am. Ceram. Soc.* **101** 4791

[5] Tanigaki K, Ogi H, Sumiya H, Kusakabe K, Nakamura N, Hirao M and Ledbetter H 2013 *Nat. Commun.* **4** 2343

[6] Tian Y J, Xu B, Yu D L, Ma Y M, Wang Y B, Jiang Y B, Hu W T, Tang C C, Gao Y F, Luo K, Zhao Z S, Wang L M, Wen B, He J L and Liu Z Y 2013 *Nature* **493** 385

[7] Zhang R F, Zhang S H, Guo Y Q, Fu Z H, Legut D, Germann T C and Veprek S 2019 *Phys. Rep.* **826** 1

[8] Zhang X X, Wang Y C, Lv J, Zhu C Y, Li Q, Zhang M, Li

Q and Ma Y M 2013 *J. Chem. Phys.* **138** 134704
[9] Tehrani A M and Brgoch J 2019 *J. Solid State Chem.* **271** 47
[10] Xu B and Tian Y J 2015 *Sci. China. Mater.* **58** 132
[11] Atabaki A H, Moazeni S, Pavanello F, Gevorgyan H, Notaros J, Alloatti L, Wade M T, Sun C, Kruger S A, Meng H Y, Qubaisi K, Wang I, Zhang B H, Khilo A, Baiocco C V, Popovic M A, Stojanovic V M and Ram R J 2018 *Nature* **560** E4
[12] Guo Q L, Di Z F, Lagally M G and Mei Y F 2018 *Mater. Sci. Eng. R* **128** 1
[13] Zhu G J, Luo W, Wang L J, Jiang W and Yang J P 2019 *J. Mater. Chem. A* **7** 24715
[14] Ogata S, Li J, Hirosaki N, Shibutani Y and Yip S 2004 *Phys. Rev. B* **70** 104104
[15] Pizzagalli L, Demenet J L and Rabier J 2009 *Phys. Rev. B* **79** 045203
[16] Roundy D and Cohen M L 2001 *Phys. Rev. B* **64** 212103
[17] Wu H, Luo X, Wen L, Sun H and Chen C 2019 *Carbon* **144** 161
[18] Zhang S H, Legut D, Fu Z H, Germann T C and Zhang R F 2018 *Carbon* **137** 156
[19] Liu C, Song X Q, Li Q, Ma Y M and Chen C F 2020 *Phys. Rev. Lett.* **124** 147001
[20] Liu C, Song X Q, Li Q, Ma Y M and Chen C F 2019 *Phys. Rev. Lett.* **123** 195504
[21] Zhang J S, Bass J D, Taniguchi T, Goncharov A F, Chang Y Y and Jacobsen S D 2011 *J. Appl. Phys.* **109** 063521
[22] Zhang Y, Sun H and Chen C 2006 *Phys. Rev. B* **73** 144115
[23] Zhang S H, Zheng X, Jin Q Q, Zheng S J, Legut D, Yu X H, Gou H Y, Fu Z H, Guo Y Q, Yan B M, Peng C, Jin C Q, Germann T C and Zhang R F 2018 *Phys. Rev. Mater.* **2** 123602
[24] Chen X Q, Niu H Y, Li D Z and Li Y Y 2011 *Intermetallics* **19** 1275
[25] Lyakhov A O and Oganov A R 2011 *Phys. Rev. B* **84** 092103
[26] Wang J T, Chen C, Mizuseki H and Kawazoe Y 2013 *Phys. Rev. Lett.* **110** 165503
[27] Olijnyk H, Sikka S K and Holzapfel W B 1984 *Phys. Lett. A* **103** 137
[28] Umeno Y and Cerny M 2008 *Phys. Rev. B* **77** 100101
[29] Guler E and Guler M 2015 *Chin. J. Phys.* **53** 195
[30] Kresse G and Furthmüller J 1996 *Phys. Rev. B* **54** 11169
[31] Kresse G and Joubert D 1999 *Phys. Rev. B* **59** 1758
[32] Ceperley D M and Alder B J 1980 *Phys. Rev. Lett.* **45** 566
[33] Perdew J P and Zunger A 1981 *Phys. Rev. B* **23** 5048
[34] Methfessel M and Paxton A T 1989 *Phys. Rev. B* **40** 3616
[35] Monkhorst H J and Pack J D 1976 *Phys. Rev. B* **13** 5188
[36] Togo A and Tanaka I 2015 *Scr. Mater.* **108** 1
[37] Maintz S, Deringer V L, Tchougréeff A L and Dronskowski R 2016 *J. Comput. Chem.* **37** 1030
[38] Nelson R, Ertural C, George J, Deringer V L, Hautier G and Dronskowski R 2020 *J. Comput. Chem.* **41** 1931
[39] Deringer V L, Tchougréeff A L and Dronskowski R 2011 *J. Phys. Chem. A* **115** 5461
[40] Dronskowski R and Blöchl P E 1993 *J. Phys. Chem.* **97** 8617
[41] Maintz S, Deringer V L, Tchougréeff A L and Dronskowski R 2013 *J. Comput. Chem.* **34** 2557
[42] Zhang S H and Zhang R F 2017 *Comput. Phys. Commun.* **220** 403
[43] Hill R 1952 *Proc. Phys. Soc. A* **65** 349
[44] Hill R 1963 *J. Mech. Phys. Solids* **11** 357
[45] Zhang S H, Fu Z H and Zhang R F 2019 *Comput. Phys. Commun.* **238** 244
[46] Guo Y Q, Zhang S H, Beyerlein I J, Legut D, Shang S L, Liu Z K and Zhang R F 2019 *Acta Mater.* **181** 423
[47] Wang N, Fu Z H, Legut D, Wei B, Germann T C and Zhang R F 2019 *Phys. Chem. Chem. Phys.* **21** 16095
[48] Zhang S H, Legut D, Germann T C, Veprek S, Zhang H J and Zhang R F 2020 *Phys. Rev. B* **101** 014104
[49] Zhang S H, Legut D and Zhang R F 2019 *Comput. Phys. Commun.* **240** 60
[50] Joos B, Ren Q and Duesbery M S 1994 *Phys. Rev. B* **50** 5890
[51] Schoeck G 2005 *Mater. Sci. Eng. A* **400–401** 7
[52] Joos B and Duesber M S 1997 *Phys. Rev. Lett.* **78** 266
[53] Blumenau A T, Jones R, Frauenheim T, Willems B, Lebedev O I, Tendeloo G V, Fisher D and Martineau P M 2003 *Phys. Rev. B* **68** 014115
[54] Kamimura Y, Edagawa K, Iskandarov A M, Osawa M, Umeno Y and Takeuchi S 2018 *Acta Mater.* **148** 355
[55] Zhang S H, Zhang Q, Liu Z R, Legut D, Germann T C, Veprek S, Zhang H J and Zhang R F 2020 *ACS Appl. Mater. Interfaces* **12** 4135
[56] Legut D, Friak M and Sob M 2007 *Phys. Rev. Lett.* **99** 016402

Supplemental Materials for

Revealing pressure-induced softening/weakening mechanism in representative covalent materials

Tengfei Xu (徐腾飞)[1, 2], Shihao Zhang (张世毫)[1, 2], Dominik Legut[3], Stan Veprek[4], and Ruifeng Zhang (张瑞丰)[1, 2, *]

[1]*School of Materials Science and Engineering, Beihang University, Beijing 100191, P. R. China*

[2]*Center for Integrated Computational Engineering (International Research Institute for Multidisciplinary Science) and Key Laboratory of High-Temperature Structural Materials & Coatings Technology (Ministry of Industry and Information Technology), Beihang University, Beijing 100191, P. R. China*

[3]*IT4Innovations, VSB-Technical University of Ostrava, 17. listopadu 2172/15, 708 00 Ostrava, Czech Republic*

[4]*Department of Chemistry, Technical University Munich, Lichtenbergstr. 4, D-85747 Garching, Germany*

* Corresponding author: zrf@buaa.edu.cn (Ruifeng Zhang)

Fig. S1. Calculated phonon dispersion curves of (a) diamond, (b) c-BN, (c) Si and (d) Ge under zero and high pressures.

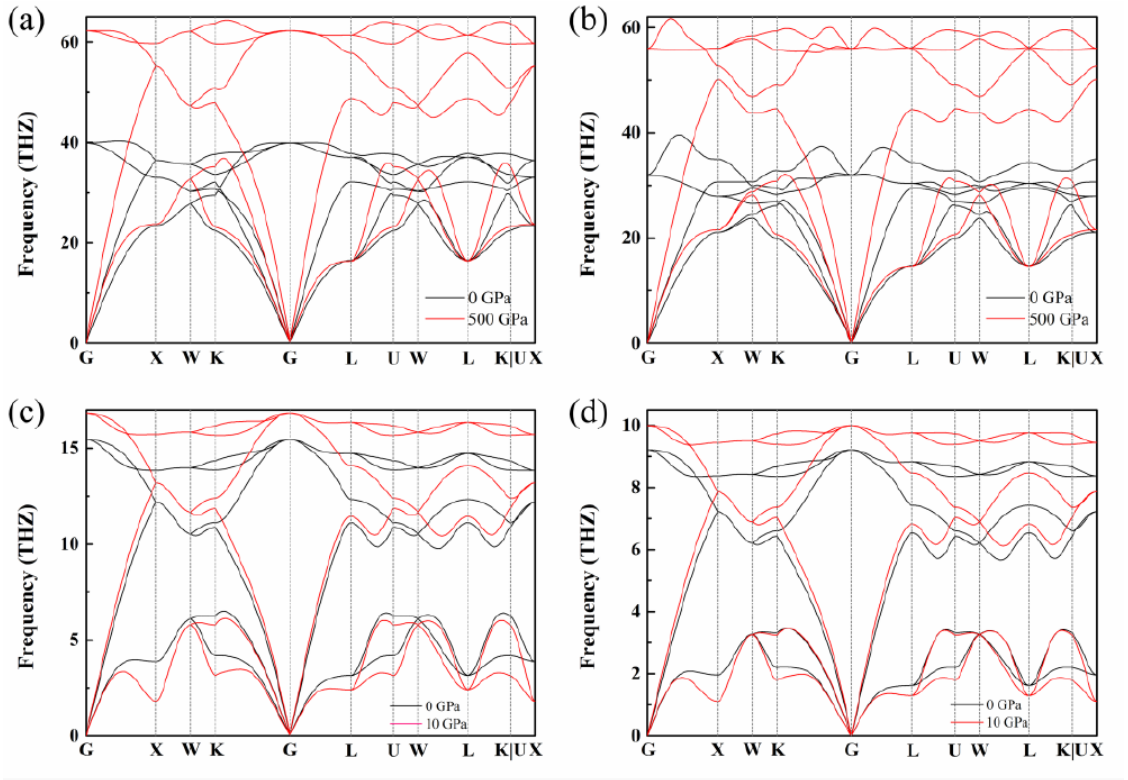

Fig. S2. Calculated isosurfaces of the VCDD of (a1)-(a9) diamond, (b1)-(b9) c-BN, (c1)-(c9) Si and (d1)-(d9) Ge under different strains along the (111)[11$\bar{2}$] shearing path under different pressures. The unit of VCDD is electrons/Bohr^3, and a same isosurface level of ±0.0305, ±0.0340, ±0.0375 electrons/Bohr^3 is used for diamond under 300, 400 and 500 GPa, ±0.022, ±0.033, ±0.036 for c-BN under 100, 400 and 500 GPa, ±0.008 for Si and ±0.005 for Ge under 0, 2, 10 GPa, respectively. Blue and yellow regions signify the states of charge depletion (negative) and accumulation (position), respectively.

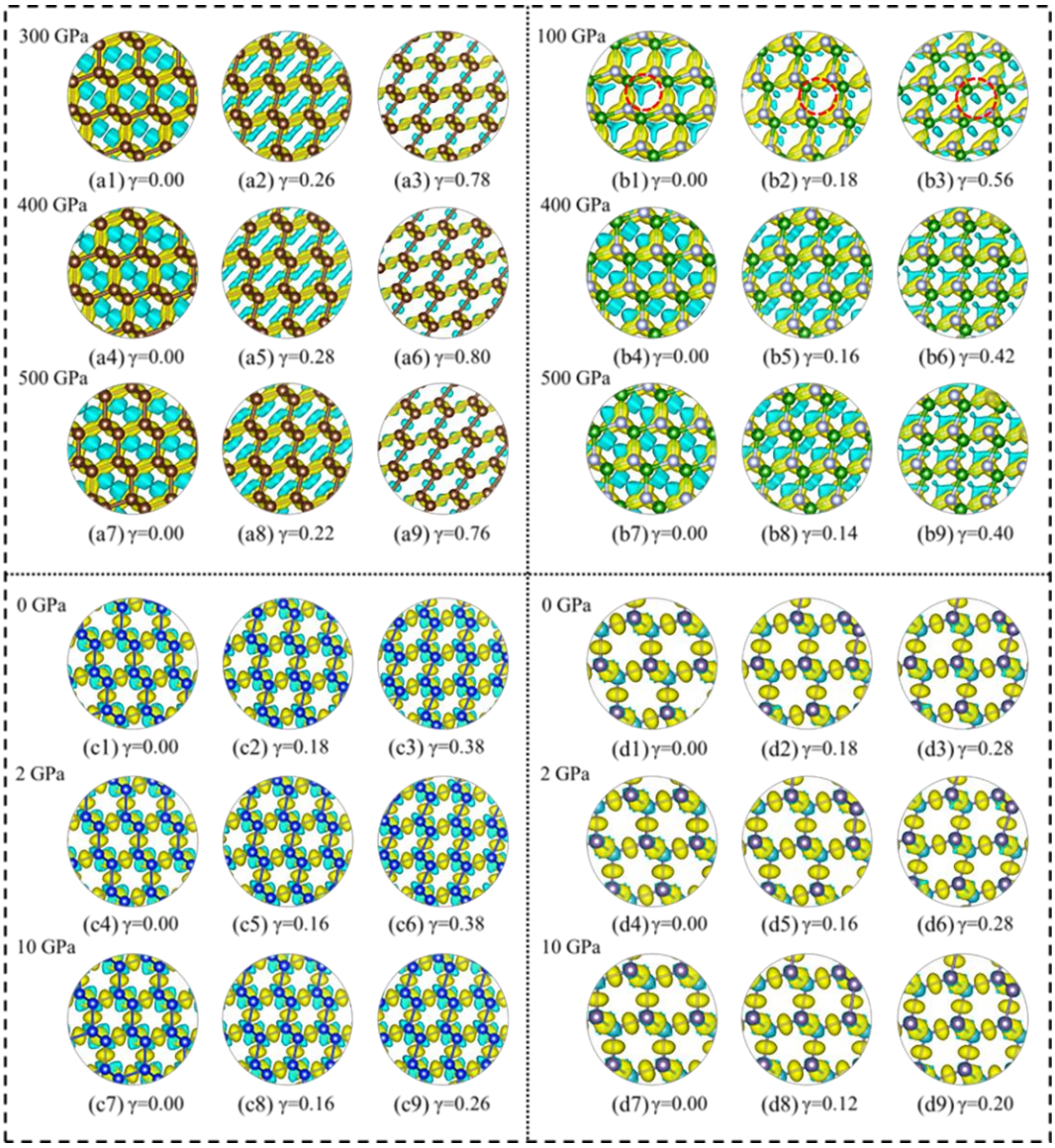

Fig. S3. Fat band structures and the corresponding DOS curves of diamond slipping with various displacements (γ=0.00, 0.45) along the shuffle-set plane at different pressures.

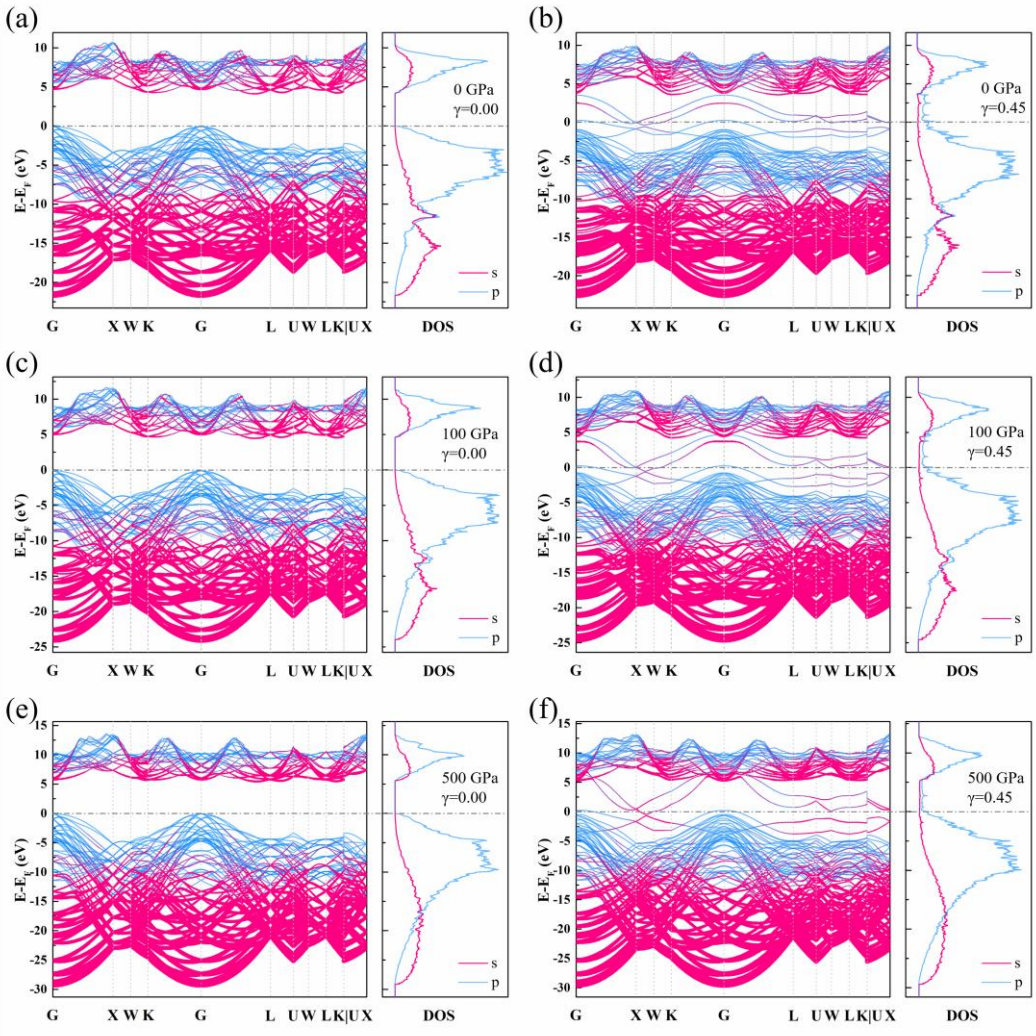

Fig. S4. The COHP curves of the bonds around the slip plane "S0" in (a) Si and (b) Ge under various displacements (u=0.00 and u=0.45) at different pressures.

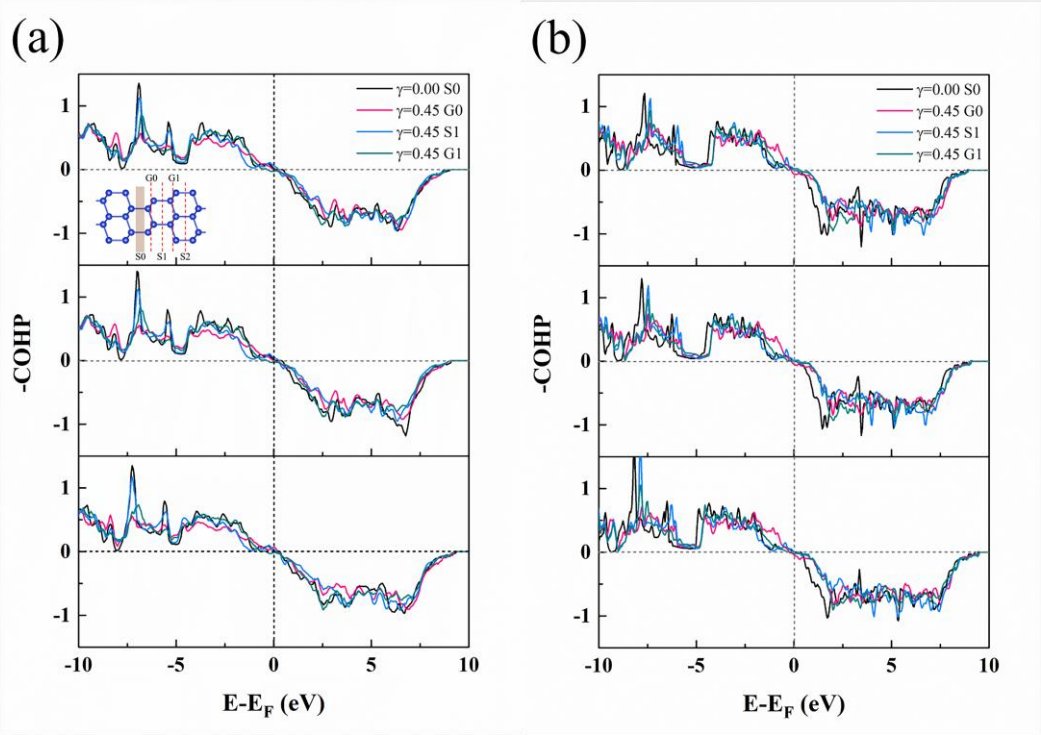

Table S1. The calculated lattice constant a (in Å), polycrystalline shear (G_{VRH}) and bulk (K_{VRH}) moduli (in GPa), Pugh ratio (G_{VRH}/B_{VRH}), ideal strength σ_{min} and τ_{min} (in GPa) under uniform strain along the weakest [111] tensile and (111)[$11\bar{2}$] shear direction, respectively, the unstable GSFEs γ_{US} (in J/m^2) and Peierls stresses τ_P (in GPa) along the [$1\bar{1}0$] and [$11\bar{2}$] directions on the shuffle-set and glide-set plane for diamond, c-BN and Si, together with the experimental data and other theoretical values for comparison.

Material	a	G_{VRH}	B_{VRH}	Pugh ratio	σ_{min}	τ_{min}	$\gamma_{US\text{-}shuffle\text{-}[1\bar{1}0]}$	$\gamma_{US\text{-}glide\text{-}[11\bar{2}]}$	$\tau_{P\text{-}shuffle\text{-}[1\bar{1}0]}$	$\tau_{P\text{-}glide\text{-}[11\bar{2}]}$
Diamond	3.535	541.34	467.85	1.157	92.33	93.2	9.97	5.77	14.3	14.8
	3.534 [1]	543.8 [1]	471.18 [1]	1.154 [1]	95 [2]	93 [2]	9.93 [1]	5.77 [3]	13.3 [3]	19.5 [3]
	3.567 [4,5]	545 [6]	468 [6]	1.165 [6]	90.7 [1]	93.9 [1,3]	9.72 [3]	5.74 [7]	13.0 [8]	
c-BN	3.583	402.73	403.22	0.999	65.4	65.3	7.47	3.76	10.83	2.83
	3.583 [1]	403.51 [1]	404.41 [1]	0.998 [1]	64.9 [3]	65.2 [3]	7.44 [3]	3.79 [3]	12.4 [3]	3.79 [3]
	3.62 [9]		400 [10]		65.9 [1]	64.9 [1]	7.20 [8]	3.43 [8]	10.3 [8]	3.73 [8]
Si	5.403	63.24	96.83	0.6531	20.97	7.25	1.45	1.82	1.3	14.28
	5.39 [11]	56.6 [12]	97.9 [13]		19.2 [8]	7.8 [8]	1.67 [14]	1.91 [14]	1.7 [8]	10-26[15]
	5.375 [12]	57.9 [11]	99.2 [8]		22 [2]	6.8 [2]		1.89 [16]	0.6-2.8 [15]	
Ge	5.65	47.12	72.35	0.6513	14.38	5.08	1.10	1.55	0.60	13.78
	5.65 [17]	46 [17]	83 [17]	0.5542 [17]	14 [2]	4.3 [2]	1.20 [18]		0.4-0.5 [18]	
	5.66 [19]	47 [19]	77 [19]	0.6104 [19]		5.4 [17]				

Reference

[1] Zhang S H, Legut D, Fu Z H, Germann T C and Zhang R F 2018 *Carbon* **137** 156

[2] Roundy D and Cohen M L 2001 *Phys. Rev. B* **64** 212103

[3] Zhang S H, Legut D, Germann T C, Veprek S, Zhang H J and Zhang R F 2020 *Phys. Rev. B* **101** 014104

[4] Straumanis M E and Aka E Z 1951 *J. Am. Chem. Soc.* **73** 5643

[5] Hom T, Kiszenik W and Post B 1975 *J. Appl. Crystallogr.* **8** 457

[6] Wang J Q, Zhao C X, Niu C Y, Sun Q and Jia Y 2016 *J. Phys. Condes. Matter* **28** 475402

[7] Zhang S H, Fu Z H and Zhang R F 2019 *Comput. Phys. Commun.* **238** 244

[8] Zhang S H, Zheng X, Jin Q Q, Zheng S J, Legut D, Yu X H, Gou H Y, Fu Z H, Guo Y Q, Yan B M, Peng C, Jin C Q, Germann T C and Zhang R F 2018 *Phys. Rev. M* **2** 123602
[9] Kern G, Kresse G and Hafner J 1999 *Phys. Rev. B* **59** 8551
[10] Grimsditch M, Zouboulis E S and Polian A 1994 *J. Appl. Phys.* **76** 832
[11] Ogata S, Li J, Hirosaki N, Shibutani Y and Yip S 2004 *Phys. Rev. B* **70** 104104
[12] Umeno Y and Kitamura T 2002 *Mater. Sci. Eng., B* **88** 79
[13] Fukumoto A 1990 *Phys. Rev. B* **42** 7462
[14] Kaxiras E and Duesbery M S 1993 *Phys. Rev. Lett.* **70** 3752
[15] Wang S, Zhang H, Wu X and Liu R 2010 *J. Phys. Condens. Matter* **22** 055801
[16] Joos B, Ren Q and Duesbery M S 1994 *Phys. Rev. B* **50** 5890
[17] Umeno Y and Cerny M 2008 *Phys. Rev. B* **77** 100101
[18] Zhang H L 2011 *Eur. Phys. J. B* **81** 179
[19] McSkimin H J 1953 *J. Appl. Phys.* **24** 988